

Accepted Manuscript

Enhanced light absorption due to the mixing state of black carbon in fresh biomass burning emissions

Qiyuan Wang, Junji Cao, Yongming Han, Jie Tian, Yue Zhang, Siwatt Pongpiachan, Yonggang Zhang, Li Li, Xinyi Niu, Zhenxing Shen, Zhuizi Zhao, Danai Tipmanee, Suratta Bunsomboonsakul, Yang Chen, Jian Sun

PII: S1352-2310(18)30133-X

DOI: [10.1016/j.atmosenv.2018.02.049](https://doi.org/10.1016/j.atmosenv.2018.02.049)

Reference: AEA 15866

To appear in: *Atmospheric Environment*

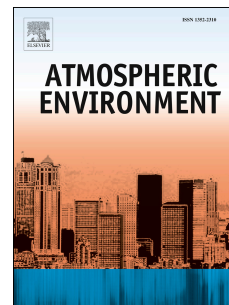
Received Date: 29 December 2017

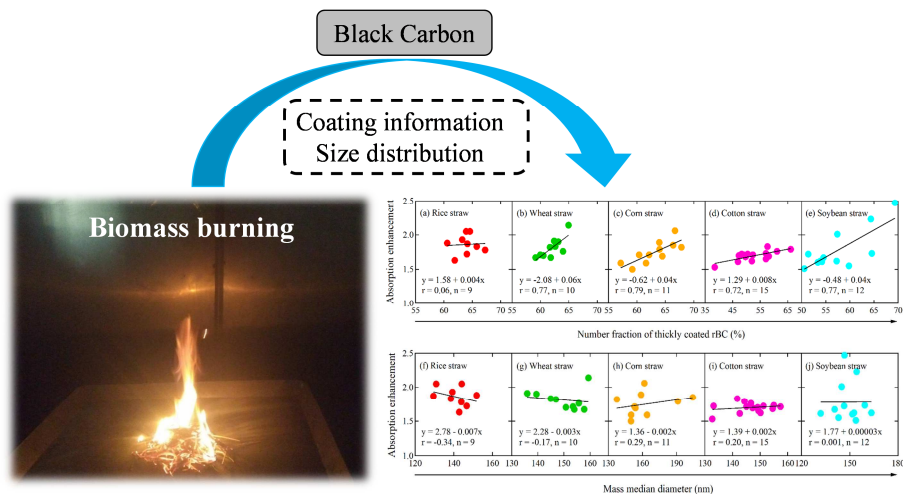
Revised Date: 21 February 2018

Accepted Date: 26 February 2018

Please cite this article as: Wang, Q., Cao, J., Han, Y., Tian, J., Zhang, Y., Pongpiachan, S., Zhang, Y., Li, L., Niu, X., Shen, Z., Zhao, Z., Tipmanee, D., Bunsomboonsakul, S., Chen, Y., Sun, J., Enhanced light absorption due to the mixing state of black carbon in fresh biomass burning emissions, *Atmospheric Environment* (2018), doi: 10.1016/j.atmosenv.2018.02.049.

This is a PDF file of an unedited manuscript that has been accepted for publication. As a service to our customers we are providing this early version of the manuscript. The manuscript will undergo copyediting, typesetting, and review of the resulting proof before it is published in its final form. Please note that during the production process errors may be discovered which could affect the content, and all legal disclaimers that apply to the journal pertain.





Graphical Abstract

1 **Enhanced light absorption due to the mixing state of black carbon in**
2 **fresh biomass burning emissions**

3 Qiyuan Wang^{1*}, Junji Cao^{1,2*}, Yongming Han^{1,3}, Jie Tian⁴, Yue Zhang⁴, Siwatt
4 Pongpiachan⁵, Yonggang Zhang¹, Li Li¹, Xinyi Niu³, Zhenxing Shen⁴, Zhuizi Zhao¹,
5 Danai Tipmanee⁶, Suratta Bunsomboonsakul⁵, Yang Chen⁷, and Jian Sun⁴

6 ¹*Key Laboratory of Aerosol Chemistry and Physics, State Key Laboratory of Loess*
7 *and Quaternary Geology, Institute of Earth Environment, Chinese Academy of*
8 *Sciences, Xi'an 710061, China*

9 ²*Institute of Global Environmental Change, Xi'an Jiaotong University, Xi'an 710049,*
10 *China*

11 ³*School of Human Settlements and Civil Engineering, Xi'an Jiaotong University, Xi'an*
12 *710049, China*

13 ⁴*Department of Environmental Science and Technology, School of Energy and Power*
14 *Engineering, Xi'an Jiaotong University, Xi'an 710049, China*

15 ⁵*School of Social & Environmental Development, National Institute of Development*
16 *Administration (NIDA), Bangkok 10240, Thailand*

17 ⁶*Faculty of Technology and Environment, Prince of Songkla University, Phuket*
18 *Campus, Kathu, Phuket 83120, Thailand*

19 ⁷*Chongqing Institute of Green and Intelligent Technology, Chinese Academy of*
20 *Sciences, Chongqing 400714, China*

21 ***Corresponding authors:** Qiyuan Wang (wangqy@ieecas.cn) and Junji Cao
22 (cao@loess.llqg.ac.cn)

23 **Keywords:** black carbon, mixing state, size distribution, light absorption, biomass
24 burning

25 **ABSTRACT**

26 A lack of information on the radiative effects of refractory black carbon (rBC)
27 emitted from biomass burning is a significant gap in our understanding of climate
28 change. A custom-made combustion chamber was used to simulate the open burning
29 of crop residues and investigate the impacts of rBC size and mixing state on the
30 particles' optical properties. Average rBC mass median diameters ranged from 141 to
31 162 nm for the rBC produced from different types of crop residues. The number
32 fraction of thickly-coated rBC varied from 53 to 64%, suggesting that a majority of
33 the freshly emitted rBC were internally mixed. By comparing the result of observed
34 mass absorption cross-section to that calculated with Mie theory, large light
35 absorption enhancement factors (1.7–1.9) were found for coated particles relative to
36 uncoated cores. These effects were strongly positively correlated with the percentage
37 of coated particles but independent of rBC core size. We suggest that rBC from open
38 biomass burning may have strong impact on air pollution and radiative forcing
39 immediately after their production.

40 1. Introduction

41 Black carbon (BC) is produced during the incomplete combustion of
42 carbon-containing materials, and it is the dominant light-absorbing form of
43 atmospheric particulate matter for visible and infrared wavelengths of light (Bond et
44 al., 2013). Light absorption by anthropogenic BC particles can perturb the Earth's
45 radiative balance and in so doing cause warming aloft and surface dimming on both
46 regional and global scales (Ramanathan and Carmichael, 2008; Booth and Bellouin,
47 2015). Climate modeling studies indicate that BC is the second largest contributor to
48 current global warming after carbon dioxide (CO₂) (Jacobson, 2001; Bond et al.,
49 2013). In addition, BC plays an important role in haze pollution through its impacts
50 on the aerosol-planetary boundary layer (Ding et al., 2016). Further, BC is associated
51 with adverse impacts on human health and crop yields (Tollefsen et al., 2009; Li et al.,
52 2016), and it also has been linked to reductions in precipitation and negative
53 influences on terrestrial and aquatic ecosystems (Forbes et al., 2006; Hodnebrog et al.,
54 2016).

55 Estimates from modeling studies indicate that the direct radiative forcing caused
56 by BC is about +0.71 W m⁻², but the uncertainty of the estimates is large, ~90%,
57 ranging from +0.08 to +1.27 W m⁻² (Bond et al., 2013). One of the difficulties in
58 making reliable estimates of BC radiative effects is that the calculations are sensitive
59 to whether the particles are treated as internally- or externally-mixed with non-BC
60 materials (Bauer et al., 2010). Furthermore, there also are still uncertainties
61 concerning the effects of BC mixing state on light absorption. Both laboratory studies
62 and field measurements have shown that particles' light absorption can be enhanced
63 by the internally-mixed BC. For example, Liu et al. (2015) demonstrated clearly that
64 coatings can substantially enhance light absorption, with the magnitude strongly
65 depending on extent of the BC coatings and their sources. Wang et al. (2014a)
66 reported an absorption enhancement of 1.8 in a polluted urban city of China due to the
67 large percentage of coated BC particles. Peng et al. (2016) found an absorption

68 amplification factor of 2.4 for BC particles after they aged several hours. In contrast,
69 however, Cappa et al. (2012) observed a small BC absorption enhancement of only 6%
70 at two sites in California, and the effect increased weakly with photochemical aging.
71 Lan et al. (2013) similarly found that coated BC particles only amplified light
72 absorption by ~7% in an urban atmosphere of South China. These discrepancies may
73 be attributed to several factors, such as particle's size, shape, and coatings as well as
74 the emission sources. Our understanding of how the BC mixing state affects the
75 particles' light absorption is still limited.

76 Biomass burning is one of the largest sources for BC in the global atmosphere
77 (Bond et al., 2013). In China, open biomass burning is an especially important
78 contributor to BC and estimated to be 137 Gg in 2013 (Qiu et al., 2016). Of the
79 biomass sources, the burning of crop residues (e.g., rice, wheat, and corn) has its most
80 significant impact on BC emissions during the summer/autumn harvest seasons. The
81 traditional method of "slash and burn" agricultural is often used to clear fields of
82 leftover plant residues and return nutrients to the soil. Although the Chinese
83 government has taken measures to prohibit the open burning of agricultural crop
84 residues, local enforcement of the regulations is still uneven. According to the
85 agricultural fire map from Zha et al. (2013), the numbers of total agricultural fire sites
86 in China were 5514 in 2009 and 4225 in 2010, and >80% of them were distributed in
87 the agricultural regions. Moreover, recent studies have shown that crop field burning
88 activities not only led to local air pollution but also had effects on regional air quality
89 through the transport and dispersal of pollutants (Long et al., 2016).

90 Studies on BC emissions from open burning of crop residues in China have been
91 presented in previous publications (Chen et al., 2017, and references therein), but
92 limited investigations have specifically focused on the effects of the BC size and
93 mixing state on particles' optical properties. In this study, a custom-made combustion
94 chamber was used to simulate the open burning of several representative types of crop
95 residues. We demonstrate substantial light absorption enhancement of refractory BC

96 (rBC) in fresh biomass-burning emissions relative to uncoated particle cores. Through
97 detailed physicochemical analyses, we show that the absorption enhancement is
98 strongly related to the amounts of coatings on the rBC particles. The results contribute
99 to our understanding of the optical properties of rBC particles produced through
100 biomass burning.

101 **2. Experimental methods**

102 **2.1. Combustion chamber experiment**

103 Test burns were conducted in a custom-made combustion chamber at the Institute
104 of Earth Environment, Chinese Academy of Sciences (IEECAS) to simulate the open
105 burning of crop residues. The combustion chamber is a $\sim 8 \text{ m}^3$ cavity container with a
106 length, width, and height of 1.8, 1.8, and 2.2 m, respectively. The chamber has 3 mm
107 thick passivated aluminum walls to withstand high combustion temperatures inside
108 the chamber. The combustion chamber is equipped with a thermocouple, a
109 thermoanemometer, and an air purification system. A dilution sampler (Model 18,
110 Baldwin Environmental Inc., Reno, NV, USA) was installed downstream of the
111 chamber to dilute the smoke before sampling. A schematic of the instrumental setups
112 of the experiments is shown in Fig. 1. Tian et al. (2015) provided a detailed
113 description of the structure and evaluation of this combustion chamber.

114 Samples of rice, wheat, corn, cotton, and soybean straw and stalks were collected
115 from seven major Chinese crop producing provinces (e.g., Shandong, Shaanxi, Hunan,
116 Henan, Hebei, Jiangxi, and Anhui), which accounted for $\sim 40\%$ of total mass of those
117 crops in China in 2015 (China Statistical Yearbook, 2016). Meanwhile, Ni et al. (2017)
118 have pointed out that there are no significant differences in $\text{PM}_{2.5}$ chemical source
119 profiles for the same crop residues from different regions. The samples were stored at
120 a stable temperature of $\sim 20 \text{ }^\circ\text{C}$ and relative humidity of 35–45% for at least one
121 month before burning. Aliquots of $\sim 52 \text{ g}$ were weighed, and the samples were burned
122 on a platform inside the combustion chamber for $\sim 5\text{--}10$ minutes. The smoke emitted

123 from each test burn was first diluted with the dilution sampler and then sampled by
124 several on-line instruments downstream. The dilution ratio was ~20–25 for most
125 burning cases. A total of 57 tests were conducted as follows: 9 for rice straw, 10 for
126 wheat straw, 11 for corn stalks, 15 for cotton stalks, and 12 for soybean stalks.
127 Detailed information on each test burn is summarized in Table 1.

128 **2.2. Quantification of rBC mass, size and mixing state**

129 The mass, size, and mixing state of rBC particles were determined with a
130 single-particle soot photometer (SP2, Droplet Measurement Technology, Boulder, CO,
131 USA), which uses a laser-induced incandescence for the measurements (Schwarz et
132 al., 2006; Gao et al., 2007). An rBC particle that enters the instrument is heated by an
133 intra-cavity Nd: YAG laser ($\lambda = 1064$ nm) to its vaporization temperature, and that
134 causes the emission of thermal radiation, which is measured by two types of optical
135 detectors. The peak incandescence signal is proportional to the rBC mass, and it is not
136 affected by the particle morphology or mixing state (Slowik et al., 2007). In this study,
137 the peak intensity of the incandescence signal was converted to rBC mass using a
138 standard fullerene soot sample (Lot F12S011, Alfa Aesar, Inc., Ward Hill, MA, USA).
139 An atomizer (Model 9302, TSI Inc., Shoreview, MN, USA) was used to generate BC
140 particles from the fullerene soot. After the particles passed through a diffusion
141 silica-gel dryer, they were size-selected with a differential mobility analyzer (Model
142 3080, TSI Inc.) before the instrumental analysis. The uncertainty of the SP2
143 measurements is ~20%. Detailed descriptions of the SP2 calibration procedures can
144 be found in our previous publications (Wang et al., 2014a; 2014b).

145 The mass-equivalent diameters of rBC cores were calculated from the measured
146 rBC masses by assuming the rBC particles were solid spheres with a density of 1.8 g
147 cm^{-3} (Bond and Bergstrom, 2006), and the values ranged from ~70 to 700 nm (see Fig.
148 2). It is important to note that the rBC core sizes measured in this way do not include
149 the contributions of non-rBC materials to the particle diameter because those
150 materials are vaporized as described above. The rBC mass fraction outside the lower

151 and upper particle size limits for the SP2 (~10%) was estimated by fitting a
152 log-normal distribution to the measured rBC mass-size distribution (Wang et al.,
153 2016a).

154 The rBC mixing state was characterized by the lag-time between the peaks of
155 incandescence and scattering signals. The lag-time occurs because coatings have to be
156 removed from the rBC core before incandescent temperatures of the cores are reached.
157 Fig. 3 shows that the lag-times displayed a bimodal distribution with ~2 μs separating
158 two distinct populations for all types of crop residues emissions. The rBC-containing
159 particles with lag-times <2 μs were classified as uncoated or thinly-coated while those
160 with lag-times >2 μs were considered to have significant amounts of coatings and
161 therefore classified as thickly-coated particles (Wang et al., 2016b). The degree of
162 rBC mixing is expressed as the number fraction of thickly-coated rBC and calculated
163 as the percentage of rBC-containing particles with lag-times >2 μs .

164 2.3. Light absorption measurements

165 The light absorption coefficient (B_{abs}) of particles was directly measured with a
166 Photoacoustic Extinctionmeter (PAX, Droplet Measurement Technologies, Boulder,
167 CO) at $\lambda = 870$ nm, which uses intracavity photoacoustic technology. A laser beam in
168 the acoustic chamber of this instrument heats the sampled light-absorbing particles,
169 and this heating produces a pressure wave that is detected with a sensitive microphone.
170 Additionally, PAX also can simultaneously measure light scattering coefficient (B_{scat})
171 with a wide-angle integrating reciprocal nephelometer in the scattering chamber.
172 Before the biomass-burning experiments, ammonium sulfate and freshly-generated
173 propane BC were used to calibrate the B_{scat} and B_{abs} , respectively. The light extinction
174 coefficient ($B_{\text{ext}} = B_{\text{scat}} + B_{\text{abs}}$) can be calculated from the laser power of the PAX;
175 thus, a correction factor can be established from the relationship between the
176 calculated B_{abs} ($= B_{\text{ext}} - B_{\text{scat}}$) and the measured B_{abs} . The equation of B_{ext} is given by:

$$177 \quad B_{\text{ext}} = -\frac{1}{0.354} \times \ln \frac{I}{I_0} \times 10^6 [\text{Mm}^{-1}] \quad (1)$$

178 where 0.354 is the path length of the laser beam through the cavity in meters; 10^6 is a
179 conversion factor to express B_{ext} in Mm^{-1} ; I_0 is the average laser power before and/or
180 after calibration; and I is the laser power during calibration. Because the scattering
181 produced by BC cannot be negligible, the B_{abs} is calculated by subtracting B_{scat} from
182 B_{ext} . The B_{scat} should be calibrated first following the same calibration steps of B_{abs} . A
183 linear relationship is then established between extinction-minus-scattering coefficient
184 and measured B_{abs} . The slope of the linear regression is used as the correction factor
185 inputted into the PAX as the new absorption factor. In this study, the same steps of
186 absorption calibration were repeated until the correction factor was stable within ~5%.

187 **2.4. Calculation of modified combustion efficiency (MCE)**

188 The combustion conditions during each test burn were characterized by
189 calculating the MCE, which is a function of the relative amounts of carbon emitted as
190 CO_2 and carbon monoxide (CO) (Kondo et al., 2011):

$$191 \quad \text{MCE} = \frac{\Delta[\text{CO}_2]}{\Delta[\text{CO}_2] + \Delta[\text{CO}]} \quad (2)$$

192 where $\Delta[\text{CO}_2]$ and $\Delta[\text{CO}]$ are the excess mixing ratios of CO_2 and CO, respectively,
193 which are calculated by subtracting the combustion chamber background, that is, the
194 air measured before ignition, from the values obtained during the test burn. Real-time
195 CO_2 and CO mixing ratios were measured with a nondispersive infrared CO_2 analyzer
196 (Model SBA-4, PP System, Amesbury, MA, USA) and a CO analyzer (Model 48i,
197 Thermo Scientific Inc. Franklin, MA, USA), respectively.

198 **3. Results and discussion**

199 **3.1. Size distributions of rBC cores**

200 The mass-equivalent diameters of the rBC cores of the burning residues were
201 well represented by mono-modal lognormal distributions (Fig. 2), and this finding is
202 consistent with previous observations from both laboratory and field biomass-burning
203 studies (Schwarz et al., 2008; May et al., 2014; Taylor et al., 2014). Fig. 4a shows the

204 distributions of rBC mass median diameters (MMDs) of each test burn for the five
205 types of crop residues emissions. The rBC MMDs were found in relatively narrow
206 ranges, varying from 129–152, 136–159, 137–204, 133–157, and 132–163 nm for rice,
207 wheat, corn, cotton, and soybean residues, respectively; with corresponding arithmetic
208 mean values (\pm standard deviation, SD), also in nm, of 141 (\pm 7), 150 (\pm 8), 162 (\pm
209 19), 147 (\pm 7), and 149 (\pm 9). The student's *t*-tests for the rBC MMDs from the
210 different types of fuels showed that there was a statistically significant difference at a
211 probability for chance occurrence of <5% ($p = 0.002$) between rice straw and corn
212 stalk emissions while the differences for other types of crop residues emissions were
213 not significant ($p = 0.15$ to 1.0).

214 The type of combustion, that is, whether the fire is flaming or smoldering, can
215 lead to distinct differences in the properties of the emitted particles (Ni et al., 2015).
216 The MCE values for the different test burns, which are a measure of how efficiently
217 the fuels are burned (Yokelson et al., 1996), ranged from ~0.79 to 0.95, and this
218 reflects the amount of variability in completeness of combustion from burn-to-burn. A
219 MCE >0.9 is characteristic of the flaming phase while a MCE <0.9 represents the
220 smoldering phase (Reid et al., 2005). Fig. 5 shows that the MMDs of the emissions
221 correlated either weakly or insignificantly with the MCEs ($r = -0.55$ to 0.27 and $p =$
222 0.08 to 0.84), suggesting that the smoldering or flaming conditions had limited effects
223 on the rBC core sizes. May et al. (2014) similarly found no clear relationship between
224 MMDs and MCEs for the burning of some individual plant species in a laboratory
225 combustion study. It should be noted that there were no test burns occurred under the
226 condition of MCE >0.95 in this study. Liu et al. (2014) reported that the single
227 scattering albedo (scattering/(absorption + scattering)) from biomass burning
228 dramatically decreased with the increasing MCE when it larger than 0.95, implying
229 that large fraction of rBC may be produced. More rBC particles favor rBC-rBC
230 coagulation, and thereby leads to increases in rBC core size. Thus, the bad correlation

231 between MMDs and MCEs in this study may be also related to the relative weak
232 rBC-rBC coagulation under MCE <0.95.

233 Compared with previous biomass-burning observations made with an SP2, our
234 average MMDs fall within the lower limits of ~140–190 nm from laboratory-based
235 biomass-burning experiments reported by May et al. (2014). However, the average
236 MMDs found in our study are considerably smaller than those for aircraft
237 measurements (altitudes: ~1.8–5.0 km) made in biomass-burning plumes in the
238 ambient atmosphere (Kondo et al., 2011; Sahu et al., 2012; Taylor et al., 2014). For
239 example, Kondo et al. (2011) found that MMDs were 177–197 nm in fresh
240 biomass-burning plumes (age <1 day) that originated from North America and 176–
241 238 nm in aged biomass-burning plumes (age: 2–3 days) from Asia. Taylor et al.
242 (2014) reported MMDs of 194 nm (age: ~1 day) and 196 nm (age: ~2 days) in two
243 biomass-burning plumes from a Canadian boreal forest. Sahu et al. (2012) observed
244 MMDs of 172–210 nm for biomass-burning plumes encountered over different
245 regions of California. In addition to the fact that different types of biomass (e.g., crop
246 residues versus various forest vegetation) can produce distinct MMDs, the larger
247 MMDs in ambient biomass-burning studies may be also related to their higher MCEs
248 compared with our laboratory study. In most cases, only an active flaming fire (e.g.,
249 MCE >0.95) can produce enough heat to convect the plume to higher altitudes, and
250 the high MCE is favor to rBC-rBC coagulation leading to relative large MMDs.
251 Moreover, another possible reason for the larger MMDs in the studies of the ambient
252 atmosphere compared with our laboratory study is that atmospheric aging/coagulation
253 processes may cause growth in rBC cores in the field as the particles in most of the
254 ambient studies were sampled a day or more after their production.

255 **3.2. Mixing State of rBC**

256 Freshly emitted rBC particles are typically externally mixed with other aerosol
257 components, but they become internally mixed through physicochemical aging
258 processes in the atmosphere (China et al., 2015). In biomass-burning plumes, rBC

259 particles are thought to become coated with other materials in the first few hours after
260 emission (Akagi et al., 2012). A more efficient burning phase (flaming; MCE >0.9)
261 will favor production of rBC relative to organic aerosol, while less efficient burning
262 condition (smoldering; MCE <0.9) will tend to produce more organic aerosol
263 compared with rBC, leading to large formation of thickly-coated rBC particles
264 (Kondo et al., 2011; Collier et al., 2016). As shown in Fig. 4b, the average number
265 fraction of thickly-coated rBC is comparable among different types of
266 biomass-burning emissions, with arithmetic means \pm SD (in %) of 64 ± 2 , 62 ± 2 , 63
267 ± 3 , 53 ± 7 , and 58 ± 6 for burning straw or stalks of rice, wheat, corn, cotton, and
268 soybean, respectively; and this shows that the rBC particles were coated even though
269 they were freshly emitted.

270 To investigate the potential influence of the MCE on rBC mixing state, the
271 number fraction of thickly-coated rBC is plotted against MCEs in Fig. 6. Except for
272 the emissions from rice straw burning, the thickly-coated rBC number fraction was
273 found to be significantly anti-correlated ($r = -0.73$ to -0.65 , $p = 0.002$ to 0.03) with the
274 MCEs. This implies that when crop residues burn in smoldering fires, more coated
275 rBC particles are produced compared with the particles produced by flaming fires.
276 The larger implication of this finding is that differences in the types of both fuels and
277 fires may affect the optical properties of the particles that are produced, and this in
278 turn could influence their impact on radiative fluxes and hence climate.

279 3.3. Light absorption enhancement

280 The mass absorption cross-section (MAC, expressed in $\text{m}^2 \text{g}^{-1}$) relates rBC mass
281 concentrations to light absorption, and it is one of the key variables used in radiative
282 transfer models (Bond et al., 2013). In our study, a MAC of rBC at $\lambda = 870 \text{ nm}$
283 (MAC_{870}) was calculated by dividing the absorption coefficient measured with the
284 PAX by the rBC mass concentration detected with the SP2 ($\text{MAC}_{870} =$
285 absorption/rBC). Fig. 7 shows that $\sim 90\%$ of the MAC_{870} values for all burning cases
286 mainly fell within a relatively narrow range of $6.5\text{--}8.5 \text{ m}^2 \text{g}^{-1}$, which are comparable

287 with the values of 5.7–8.3 m² g⁻¹ that are influenced by biomass-burning emissions in
288 previous studies (Kondo et al., 2009; Subramanian et al., 2010; Laborde et al., 2013;
289 Wang et al., 2015). Average MAC₈₇₀ (± SD) for the rBC particles from rice, wheat,
290 corn, cotton, and soybean burning were 7.6 ± 0.5, 7.5 ± 0.6, 7.2 ± 0.6, 7.0 ± 0.3, and
291 7.4 ± 1.3 m² g⁻¹, respectively. The *t*-tests showed that the differences in MAC₈₇₀
292 among the various crop types were not statistically significant at a probability of 5%
293 (*p* = 0.06), suggesting that the absorption capacity of the rBC normalized by mass was
294 independent on the type of plant matter burned.

295 Based on the assumption of spherical for uncoated rBC particles, Mie theory was
296 used to calculate the MAC₈₇₀ of uncoated rBC particles (MAC_{870,uncoated}) using the
297 core sizes of rBC measured with the SP2. More details regarding the Mie algorithms
298 can be found in Bohren and Huffman (2008). For uncoated rBC, we used a refractive
299 index of 1.85 - 0.71*i* at λ = 550 nm, which is in the middle of the range suggested by
300 Bond and Bergstrom (2006). Mie theory was first applied to estimate the MAC values
301 of uncoated rBC at λ = 550 nm, and then those values were converted to
302 MAC_{870,uncoated} based on an rBC absorption Ångström exponent of 1.0 (Lack and
303 Langridge, 2013). The average absorption enhancement was calculated by comparing
304 MAC₈₇₀ for rBC with and without coatings (Enhancement = MAC₈₇₀/MAC_{870,uncoated}).

305 Large absorption enhancements were found in the fresh biomass-burning
306 emissions, with average values of 1.9 ± 0.1, 1.8 ± 0.1, 1.7 ± 0.2, 1.7 ± 0.1, and 1.8 ±
307 0.3 for straw or stalks of rice, wheat, corn, cotton, and soybean emissions,
308 respectively (Fig. 4c). These observations suggest that light absorption for relatively
309 fresh rBC is enhanced compared with that for uncoated particles. The refractive index
310 of rBC is a key input parameter in the Mie model, and we bounded our calculations
311 using the lowest (1.75-0.63*i*) and highest (1.95-0.79*i*) refractive index values
312 suggested by Bond and Bergstrom (2006). This was done to evaluate the sensitivity of
313 absorption enhancement calculations to the parameterization of the refractive index,

314 and the results show that the difference between the two extreme cases was within
315 ~15%.

316 To further investigate the potential impacts of rBC morphology and mixing state
317 on light absorption, we plotted the absorption enhancement values against the number
318 fraction of thickly-coated rBC and against the MMDs. As shown in Fig. 8(a–e),
319 except for the rice straw case, absorption enhancement was positively correlated ($r =$
320 0.72 to 0.79 , and $p = 0.003$ to 0.009) with the number fraction of thickly-coated rBC,
321 suggesting that the magnitude of the light absorption enhancement was strongly
322 affected by the amounts of coatings on the particles. There is a good explanation for
323 this; that is, light absorption caused by coated rBC is “enhanced” because the coatings
324 act as a lens that refracts more light to the particle’s core, which is called “lensing
325 effects” (Lack and Cappa, 2010). Previous studies have shown that even if for the
326 same amount of coatings, BC embedded within a particle of non-BC compounds can
327 cause larger enhancement for MAC than the one attached to the surface of a non-BC
328 particle (Fuller et al., 1999; Scarnato et al., 2013). The poor correlation for rice straw
329 emissions here may be due to the different internal morphology of rBC compared with
330 other crop residues emissions. However, this speculation needs further evidence in the
331 future work. In addition to the coating amount, the rBC core size may also affect the
332 absorption enhancement, because it provides a surface area to receive the incident
333 light. Fig. 8(f–j) shows that there was no clear relationship between absorption
334 enhancement and MMDs, suggesting that the absorption enhancement of coated rBC
335 particles is independent of the rBC core size at the range of ~129–204 nm. Thus, light
336 absorption enhancement of rBC-containing particles is apparently affected by the
337 “lensing effects” of the coatings.

338 **4. Conclusions and atmospheric implications**

339 We investigated the physicochemical properties of rBC particles produced in
340 laboratory studies of open biomass burning, and one main focus of this work was on
341 the optical properties of the particles and how they were affected by coatings on the

342 particles. Our results showed that average rBC core size ranged from 141 to 162 nm
343 for different types of crop residues emissions regardless of whether the fires were in
344 the smoldering or flaming phase. Large number fractions of thickly-coated rBC (53–
345 64%) were found in the freshly emitted particles. Smoldering crop residues tended to
346 produce more coated rBC than flaming fires. The average rBC MAC_{870} for different
347 kinds of crop residues varied from 7.0 to 7.6 $m^2 g^{-1}$. The *t*-tests showed that light
348 absorption capacity of the rBC particles was independent of the types of crop residues
349 that were burned. By comparing the result of observed MAC_{870} with SP2 and PAX to
350 that calculated with the Mie theory, it indicated that freshly emitted biomass-burning
351 rBC particles had large light absorption enhancements compared with uncoated
352 particles, with values of 1.7–1.9. The absorption enhancements were positively
353 correlation with the number fraction of thickly-coated rBC, but there was no clear
354 relationship with the rBC core size. This implies that absorption enhancement of
355 internally-mixed rBC is the result of “lensing effects” caused by the coatings.

356 For this study, there are at least three key implications for our findings (1) the
357 open burning of crop residues may cause strong positive direct radiative forcing
358 immediately after their production because a large fraction of the freshly emitted rBC
359 particles have substantial coatings that cause increased light absorption; (2) the
360 enhanced optical properties of rBC could contribute in significant ways to
361 stabilization atmosphere through heating in the planetary boundary layer and in so
362 doing depress the development of the planetary boundary layer which could increase
363 the likelihood and severity of haze events; and (3) the presence of coatings and large
364 absorption enhancement in rBC from fresh biomass-burning emissions implies that
365 atmospheric aging may have limited effects on rBC light absorption although changes
366 in the chemical composition of coatings with time could still affect how the particles
367 interact with light. Each of these topics will be important for further research on the
368 effects of biomass-burning emissions on the Earth’s radiative balance and climate.

369 **Acknowledgments**

370 This study was supported by the National Natural Science Foundation of China
371 (41230641, 41503118, 41661144020, and 41625015) and China Postdoctoral Science
372 Foundation (2015M580890).

373 **References**

- 374 Akagi, S.K., Craven, J.S., Taylor, J.W., McMeeking, G.R., Yokelson, R.J., Burling,
375 I.R., Urbanski, S.P., Wold, C.E., Seinfeld, J.H., Coe, H., Alvarado, M.J., Weise,
376 D.R., 2012. Evolution of trace gases and particles emitted by a chaparral fire in
377 California. *Atmos. Chem. Phys.* 12, 1397–1421,
378 <https://doi.org/10.5194/acp-12-1397-2012>.
- 379 Bauer, S.E., Menon, S., Koch, D., Bond, T.C., Tsigaridis, K., 2010. A global modeling
380 study on carbonaceous aerosol microphysical characteristics and radiative effects.
381 *Atmos. Chem. Phys.* 10, 7439–7456, <https://doi.org/10.5194/acp-10-7439-2010>.
- 382 Bohren, C.F., Huffman, D.R., 2008. Absorption and scattering of light by small
383 particles. John Wiley & Sons, New York.
- 384 Bond, T.C., Bergstrom, R.W., 2006. Light absorption by carbonaceous particles: An
385 investigative review. *Aerosol Sci. Technol.* 40, 27–67,
386 <https://doi.org/10.1080/02786820500421521>.
- 387 Bond, T.C., Doherty, S.J., Fahey, D.W., Forster, P.M., Berntsen, T., DeAngelo, B.J.,
388 Flanner, M.G., Ghan, S., Karcher, B., Koch, D., Kinne, S., Kondo, Y., Quinn,
389 P.K., Sarofim, M.C., Schultz, M.G., Schulz, M., Venkataraman, C., Zhang, H.,
390 Zhang, S., Bellouin, N., Guttikunda, S.K., Hopke, P.K., Jacobson, M.Z., Kaiser,
391 J.W., Klimont, Z., Lohmann, U., Schwarz, J.P., Shindell, D., Storelvmo, T.,
392 Warren, S.G., Zender, C.S., 2013. Bounding the role of black carbon in the
393 climate system: A scientific assessment. *J. Geophys. Res.-Atmos.* 118, 5380–
394 5552, doi:10.1002/jgrd.50171.
- 395 Booth, B., Bellouin, N., 2015. Climate change: Black carbon and atmospheric
396 feedbacks. *Nature* 519, 167–168, doi:10.1038/519167a.

- 397 Cappa, C.D., Onasch, T.B., Massoli, P., Worsnop, D.R., Bates, T.S., Cross, E.S.,
398 Davidovits, P., Hakala, J., Hayden, K.L., Jobson, B.T., Kolesar, K.R., Lack, D.A.,
399 Lerner, B.M., Li, S.-M., Mellon, D., Nuaaman, I., Olfert, J.S., Petaja, T., Quinn,
400 P.K., Song, C., Subramanian, R., Williams, E.J., Zaveri, R.A., 2012. Radiative
401 absorption enhancements due to the mixing state of atmospheric black carbon.
402 *Science* 337, 1078–1081, doi: 10.1126/science.1223447.
- 403 Chen, J., Li, C., Ristovski, Z., Milic, A., Gu, Y., Islam, M.S., Wang, S., Hao, J., Zhang,
404 H., He, C., Guo, H., Fu, H., Miljevic, B., Morawska, L., Phong, T., Fat, Y.L.A.M.,
405 Pereira, G., Ding, A., Huang, X., Dumka, U.C., 2017. A review of biomass
406 burning: Emissions and impacts on air quality, health and climate in China. *Sci.*
407 *Total Environ.* 579, 1000–1034, <https://doi.org/10.1016/j.scitotenv.2016.11.025>.
- 408 China, S., Scarnato, B., Owen, R.C., Zhang, B., Ampadu, M.T., Kumar, S., Dzepina,
409 K., Dziobak, M.P., Fialho, P., Perlinger, J.A., Hueber, J., Helmig, D., Mazzoleni,
410 L.R., Mazzoleni, C., 2015. Morphology and mixing state of aged soot particles at
411 a remote marine free troposphere site: Implications for optical properties.
412 *Geophys. Res. Lett.* 42, 1243–1250, doi: 10.1002/2014GL062404.
- 413 China Statistical Yearbook, 2016, <http://www.stats.gov.cn/tjsj/ndsj/2016/indexch.htm>.
- 414 Collier, S., Zhou, S., Onasch, T.B., Jaffe, D.A., Kleinman, L., Sedlacek, A.J., Briggs,
415 N.L., Hee, J., Fortner, E., Shilling, J.E., Worsnop, D., Yokelson, R.J., Parworth,
416 C., Ge, X.L., Xu, J.Z., Butterfield, Z., Chand, D., Dubey, M.K., Pekour, M.S.,
417 Springston, S., Zhang, Q., 2016. Regional influence of aerosol emissions from
418 wildfires driven by combustion efficiency: Insights from the BBOP campaign.
419 *Environ. Sci. Technol.* 50, 8613–8622, doi: 10.1021/acs.est.6b01617.
- 420 Ding, A.J., Huang, X., Nie, W., Sun, J.N., Kerminen, V.M., Petaja, T., Su, H., Cheng,
421 Y.F., Yang, X.Q., Wang, M.H., Chi, X.G., Wang, J.P., Virkkula, A., Guo, W.D.,
422 Yuan, J., Wang, S.Y., Zhang, R.J., Wu, Y.F., Song, Y., Zhu, T., Zilitinkevich, S.,
423 Kulmala, M., Fu, C.B., 2016. Enhanced haze pollution by black carbon in

- 424 megacities in China. *Geophys. Res. Lett.* 43, 2873–2879, doi:
425 10.1002/2016GL067745.
- 426 Forbes, M.S., Raison, R.J., Skjemstad, J.O., 2006. Formation, transformation and
427 transport of black carbon (charcoal) in terrestrial and aquatic ecosystems. *Sci.*
428 *Total Environ.* 370, 190–206, <https://doi.org/10.1016/j.scitotenv.2006.06.007>.
- 429 Fuller, K.A., Malm, W.C., Kreidenweis, S.M., 1999. Effects of mixing on extinction
430 by carbonaceous particles. *J. Geophys. Res.* 104, 15941–15954, doi:
431 10.1029/1998JD100069.
- 432 Gao, R.S., Schwarz, J.P., Kelly, K.K., Fahey, D.W., Watts, L.A., Thompson, T.L.,
433 Spackman, J.R., Slowik, J.G., Cross, E.S., Han, J.H., Davidovits, P., Onasch,
434 T.B., Worsnop, D.R., 2007. A novel method for estimating light-scattering
435 properties of soot aerosols using a modified single-particle soot photometer.
436 *Aerosol Sci. Technol.* 41, 125–135, <https://doi.org/10.1080/02786820601118398>.
- 437 Hodnebrog, O., Myhre, G., Forster, P.M., Sillmann, J., Samset, B.H., 2016. Local
438 biomass burning is a dominant cause of the observed precipitation reduction in
439 southern Africa. *Nat. Commun.* 7, doi:10.1038/ncomms11236.
- 440 Jacobson, M.Z., 2001. Strong radiative heating due to the mixing state of black carbon
441 in atmospheric aerosols. *Nature* 409, 695–697, doi:10.1038/35055518.
- 442 Kondo, Y., Sahu, L., Kuwata, M., Miyazaki, Y., Takegawa, N., Moteki, N., Imaru, J.,
443 Han, S., Nakayama, T., Oanh, N.T.K., Hu, M., Kim, Y.J., Kita, K., 2009.
444 Stabilization of the mass absorption cross section of black carbon for filter-based
445 absorption photometry by the use of a heated inlet. *Aerosol Sci. Technol.* 43,
446 741–756, <https://doi.org/10.1080/02786820902889879>.
- 447 Kondo, Y., Matsui, H., Moteki, N., Sahu, L., Takegawa, N., Kajino, M., Zhao, Y.,
448 Cubison, M.J., Jimenez, J.L., Vay, S., Diskin, G.S., Anderson, B., Wisthaler, A.,
449 Mikoviny, T., Fuelberg, H.E., Blake, D.R., Huey, G., Weinheimer, A.J., Knapp,
450 D.J., Brune, W.H., 2011. Emissions of black carbon, organic, and inorganic

- 451 aerosols from biomass burning in North America and Asia in 2008. *J. Geophys.*
452 *Res.-Atmos.* 116, D08204, doi:10.1029/2010JD015152.
- 453 Laborde, M., Crippa, M., Tritscher, T., Jurányi, Z., Decarlo, P.F., Temime-Roussel, B.,
454 Marchand, N., Eckhardt, S., Stohl, A., Baltensperger, U., Prévôt, A.S.H.,
455 Weingartner, E., Gysel, M., 2013. Black carbon physical properties and mixing
456 state in the European megacity Paris. *Atmos. Chem. Phys.* 13, 5831-5856,
457 <https://doi.org/10.5194/acp-13-5831-2013>.
- 458 Lack, D.A., Cappa, C.D., 2010. Impact of brown and clear carbon on light absorption
459 enhancement, single scatter albedo and absorption wavelength dependence of
460 black carbon. *Atmos. Chem. Phys.* 10, 4207-4220,
461 <https://doi.org/10.5194/acp-10-4207-2010>.
- 462 Lack, D.A., Langridge, J.M., 2013. On the attribution of black and brown carbon light
463 absorption using the Angstrom exponent. *Atmos. Chem. Phys.* 13, 10535-10543,
464 <https://doi.org/10.5194/acp-13-10535-2013>.
- 465 Lan, Z.-J., Huang, X.-F., Yu, K.-Y., Sun, T.-L., Zeng, L.-W., Hu, M., 2013. Light
466 absorption of black carbon aerosol and its enhancement by mixing state in an
467 urban atmosphere in South China. *Atmos. Environ.* 69, 118-123,
468 <https://doi.org/10.1016/j.atmosenv.2012.12.009>.
- 469 Li, Y., Henze, D.K., Jack, D., Henderson, B.H., Kinney, P.L., 2016. Assessing public
470 health burden associated with exposure to ambient black carbon in the United
471 States. *Sci. Total Environ.* 539, 515-525,
472 <https://doi.org/10.1016/j.scitotenv.2015.08.129>.
- 473 Liu, S., Aiken, A.C., Arata, C., Dubey, M.K., Stockwell, C.E., Yokelson, R.J., Stone,
474 E.A., Jayarathne, T., Robinson, A.L., DeMott, P.J., Kreidenweis, S.M., 2014.
475 Aerosol single scattering albedo dependence on biomass combustion efficiency:
476 Laboratory and field studies. *Geophys. Res. Lett.* 41(2), 742-748, doi:
477 10.1002/2013GL058392.

- 478 Liu, S., Aiken, A.C., Gorkowski, K., Dubey, M.K., Cappa, C.D., Williams, L.R.,
479 Herndon, S.C., Massoli, P., Fortner, E.C., Chhabra, P.S., Brooks, W.A., Onasch,
480 T.B., Jayne, J.T., Worsnop, D.R., China, S., Sharma, N., Mazzoleni, C., Xu, L.,
481 Ng, N.L., Liu, D., Allan, J.D., Lee, J.D., Fleming, Z.L., Mohr, C., Zotter, P.,
482 Szidat, S., Prevot, A.S.H., 2015. Enhanced light absorption by mixed source
483 black and brown carbon particles in UK winter. *Nat. Commun.* 6,
484 doi:10.1038/ncomms9435.
- 485 Long, X., Tie, X., Cao, J., Huang, R., Feng, T., Li, N., Zhao, S., Tian, J., Li, G., Zhang,
486 Q., 2016. Impact of crop field burning and mountains on heavy haze in the North
487 China Plain: a case study. *Atmos. Chem. Phys.* 16, 9675–9691,
488 <https://doi.org/10.5194/acp-16-9675-2016>.
- 489 May, A.A., McMeeking, G.R., Lee, T., Taylor, J.W., Craven, J.S., Burling, I., Sullivan,
490 A.P., Akagi, S., Collett, J.L., Jr., Flynn, M., Coe, H., Urbanski, S.P., Seinfeld,
491 J.H., Yokelson, R.J., Kreidenweis, S.M., 2014. Aerosol emissions from
492 prescribed fires in the United States: A synthesis of laboratory and aircraft
493 measurements. *J. Geophys. Res.-Atmos.* 119, 11826–11849, doi:
494 10.1002/2014JD021848.
- 495 Ni, H., Han, Y., Cao, J., Chen, L.W.A., Tian, J., Wang, X., Chow, J.C., Watson, J.G.,
496 Wang, Q., Wang, P., Li, H., Huang, R.-J., 2015. Emission characteristics of
497 carbonaceous particles and trace gases from open burning of crop residues in
498 China. *Atmos. Environ.* 123, 399–406,
499 <https://doi.org/10.1016/j.atmosenv.2015.05.007>.
- 500 Peng, J., Hu, M., Guo, S., Du, Z., Zheng, J., Shang, D., Zamora, M.L., Zeng, L., Shao,
501 M., Wu, Y.-S., Zheng, J., Wang, Y., Glen, C.R., Collins, D.R., Molina, M.J.,
502 Zhang, R., 2016. Markedly enhanced absorption and direct radiative forcing of
503 black carbon under polluted urban environments. *Proc. Natl. Acad. Sci. U. S. A.*
504 113, 4266–4271, <https://doi.org/10.1073/pnas.1602310113>.

- 505 Qiu, X., Duan, L., Chai, F., Wang, S., Yu, Q., Wang, S., 2016. Deriving
506 high-resolution emission inventory of open biomass burning in China based on
507 satellite observations. *Environ. Sci. Technol.* 50, 11779–11786, doi:
508 10.1021/acs.est.6b02705.
- 509 Ramanathan, V., Carmichael, G., 2008. Global and regional climate changes due to
510 black carbon. *Nat. Geosci.* 1, 221–227, doi:10.1038/ngeo156.
- 511 Reid, J.S., Koppmann, R., Eck, T.F., Eleuterio, D.P., 2005. A review of biomass
512 burning emissions part II: intensive physical properties of biomass burning
513 particles. *Atmos. Chem. Phys.* 5, 799–825,
514 <https://doi.org/10.5194/acp-5-799-2005>.
- 515 Sahu, L.K., Kondo, Y., Moteki, N., Takegawa, N., Zhao, Y., Cubison, M.J., Jimenez,
516 J.L., Vay, S., Diskin, G.S., Wisthaler, A., Mikoviny, T., Huey, L.G., Weinheimer,
517 A.J., Knapp, D.J., 2012. Emission characteristics of black carbon in
518 anthropogenic and biomass burning plumes over California during
519 ARCTAS-CARB 2008. *J. Geophys. Res.-Atmos.* 117, D16302,
520 doi:10.1029/2011JD017401.
- 521 Scarnato, B.V., Vahidinia, S., Richard, D.T., Kirchstetter, T.W., 2013. Effects of
522 internal mixing and aggregate morphology on optical properties of black carbon
523 using a discrete dipole approximation model. *Atmos. Chem. Phys.* 13, 5089–
524 5101, <https://doi.org/10.5194/acp-13-5089-2013>.
- 525 Schwarz, J.P., Gao, R.S., Fahey, D.W., Thomson, D.S., Watts, L.A., Wilson, J.C.,
526 Reeves, J.M., Darbeheshti, M., Baumgardner, D.G., Kok, G.L., Chung, S.H.,
527 Schulz, M., Hendricks, J., Lauer, A., Kaercher, B., Slowik, J.G., Rosenlof, K.H.,
528 Thompson, T.L., Langford, A.O., Loewenstein, M., Aikin, K.C., 2006.
529 Single-particle measurements of midlatitude black carbon and light-scattering
530 aerosols from the boundary layer to the lower stratosphere. *J. Geophys.*
531 *Res.-Atmos.* 111, D16207, doi:10.1029/2006jd007076.

- 532 Schwarz, J.P., Gao, R.S., Spackman, J.R., Watts, L.A., Thomson, D.S., Fahey, D.W.,
533 Ryerson, T.B., Peischl, J., Holloway, J.S., Trainer, M., Frost, G.J., Baynard, T.,
534 Lack, D.A., de Gouw, J.A., Warneke, C., Del Negro, L.A., 2008. Measurement of
535 the mixing state, mass, and optical size of individual black carbon particles in
536 urban and biomass burning emissions. *Geophys. Res. Lett.* 35(13), L13810,
537 doi:10.1029/2008gl033968..
- 538 Slowik, J.G., Cross, E.S., Han, J.-H., Davidovits, P., Onasch, T.B., Jayne, J.T.,
539 WilliamS, L.R., Canagaratna, M.R., Worsnop, D.R., Chakrabarty, R.K.,
540 Moosmueller, H., Arnott, W.P., Schwarz, J.P., Gao, R.-S., Fahey, D.W., Kok, G.L.,
541 Petzold, A., 2007. An inter-comparison of instruments measuring black carbon
542 content of soot particles. *Aerosol Sci. Technol.* 41, 295–314,
543 <https://doi.org/10.1080/02786820701197078>.
- 544 Subramanian, R., Kok, G.L., Baumgardner, D., Clarke, A., Shinozuka, Y., Campos,
545 T.L., Heizer, C.G., Stephens, B.B., de Foy, B., Voss, P.B., Zaveri, R.A., 2010.
546 Black carbon over Mexico: the effect of atmospheric transport on mixing state,
547 mass absorption cross-section, and BC/CO ratios. *Atmos. Chem. Phys.* 10,
548 219-237, <https://doi.org/10.5194/acp-10-219-2010>.
- 549 Taylor, J.W., Allan, J.D., Allen, G., Coe, H., Williams, P.I., Flynn, M.J., Le Breton, M.,
550 Muller, J.B.A., Percival, C.J., Oram, D., Forster, G., Lee, J.D., Rickard, A.R.,
551 Parrington, M., Palmer, P.I., 2014. Size-dependent wet removal of black carbon
552 in Canadian biomass burning plumes. *Atmos. Chem. Phys.* 14, 13755–13771,
553 <https://doi.org/10.5194/acp-14-13755-2014>.
- 554 Tian, J., Chow, J.C., Cao, J., Han, Y., Ni, H., Chen, L.W.A., Wang, X., Huang, R.,
555 Moosmueller, H., Watson, J.G., 2015. A biomass combustion chamber: design,
556 evaluation, and a case study of wheat straw combustion emission tests. *Aerosol*
557 *Air Qual. Res.* 15, 2104–2114, doi: 10.4209/aaqr.2015.03.0167.
- 558 Tollefsen, P., Rypdal, K., Torvanger, A., Rive, N., 2009. Air pollution policies in
559 Europe: efficiency gains from integrating climate effects with damage costs to

- 560 health and crops. *Environ. Sci. Policy* 12, 870–881,
561 <https://doi.org/10.1016/j.envsci.2009.08.006>.
- 562 Wang, Q., Huang, R.-J., Zhao, Z., Cao, J., Ni, H., Tie, X., Zhao, S., Su, X., Han, Y.,
563 Shen, Z., Wang, Y., Zhang, N., Zhou, Y., Corbin, J.C., 2016a. Physicochemical
564 characteristics of black carbon aerosol and its radiative impact in a polluted
565 urban area of China. *J. Geophys. Res.-Atmos.* 121, 12505–12519, doi:
566 10.1002/2016JD024748.
- 567 Wang, Q., Huang, R.-J., Zhao, Z., Zhang, N., Wang, Y., Ni, H., Tie, X., Han, Y.,
568 Zhuang, M., Wang, M., Zhang, J., Zhang, X., Dusek, U., Cao, J., 2016b. Size
569 distribution and mixing state of refractory black carbon aerosol from a coastal
570 city in South China. *Atmo. Res.* 181, 163–171,
571 <https://doi.org/10.1016/j.atmosres.2016.06.022>.
- 572 Wang, Q., Huang, R.J., Cao, J., Han, Y., Wang, G., Li, G., Wang, Y., Dai, W., Zhang,
573 R., Zhou, Y., 2014a. Mixing state of black carbon aerosol in a heavily polluted
574 urban area of China: implications for light absorption enhancement. *Aerosol Sci.*
575 *Technol.* 48, 689–697, <https://doi.org/10.1080/02786826.2014.917758>.
- 576 Wang, Q., Schwarz, J.P., Cao, J., Gao, R., Fahey, D.W., Hu, T., Huang, R.J., Han, Y.,
577 Shen, Z., 2014b. Black carbon aerosol characterization in a remote area of
578 Qinghai-Tibetan Plateau, western China. *Sci. Total Environ.* 479, 151–158,
579 <https://doi.org/10.1016/j.scitotenv.2014.01.098>.
- 580 Wang, Q.Y., Huang, R.J., Cao, J.J., Tie, X.X., Ni, H.Y., Zhou, Y.Q., Han, Y.M., Hu,
581 T.F., Zhu, C.S., Feng, T., Li, N., Li, J.D., 2015. Black carbon aerosol in winter
582 northeastern Qinghai–Tibetan Plateau, China: the source, mixing state and
583 optical property. *Atmos. Chem. Phys.* 15, 13059–13069,
584 <https://doi.org/10.5194/acp-15-13059-2015>.
- 585 Yokelson, R.J., Griffith, D.W.T., Ward, D.E., 1996. Open-path Fourier transform
586 infrared studies of large-scale laboratory biomass fires. *J. Geophys. Res.-Atmos.*
587 101, 21067–21080, doi: 10.1029/96JD01800.

588 Zha, S., Zhang, S., Cheng, T., Chen, J., Huang, G., Li, X., Wang, Q., 2013.
589 Agricultural fires and their potential impacts on regional air quality over China.
590 Aerosol Air Qual. Res. 13, 992–1001, doi: 10.4209/aaqr.2012.10.0277.
591

ACCEPTED MANUSCRIPT

592

Table 1. Summary experiments of open burning of crop residues.

Crop residues	Crop producing province	Test number	Weight (g)	Dilution ratio	Combustion time (min)
Rice straw	Anhui, Hunan, Shandong, and Jiangxi	9	50.2–55.3	20–26	4–8
Wheat straw	Henan and Shaanxi	10	51.2–53.5	20–25	7–9
Corn stalk	Hebei, Henan, Hunan, Shandong, and Shaanxi	11	50.1–55.2	22–25	5–9
Cotton stalk	Anhui, Henan, Hunan, and Shandong	15	53.1–56.7	26–38	4–12
Soybean stalk	Anhui, Henan, Hunan, and Shaanxi	12	51.6–57.7	15–35	4–10

593

594 **Figure Captions**

595 **Fig. 1.** Schematic of the instrumental setups of the experiments.

596 **Fig. 2.** Average mass size distributions of rBC in volume equivalent diameters for
597 different crop residues emissions. The solid lines represent single mode
598 lognormal fits.

599 **Fig. 3.** Frequency distributions of the incandescence lag-times for $\sim 1.1 \times 10^4$ – 1.5×10^4
600 arbitrary-selected rBC particles from different types of crop residues emissions.
601 The light grey and light yellow regions represent the uncoated or thinly-coated
602 rBC particles and the thickly-coated ones, respectively.

603 **Fig. 4.** Distributions of (a) rBC mass median diameter (MMD), (b) number fraction of
604 thickly-coated rBC (F_{rBC}), and (c) light absorption enhancement (E_{abs}) for
605 different types of crop residues emissions.

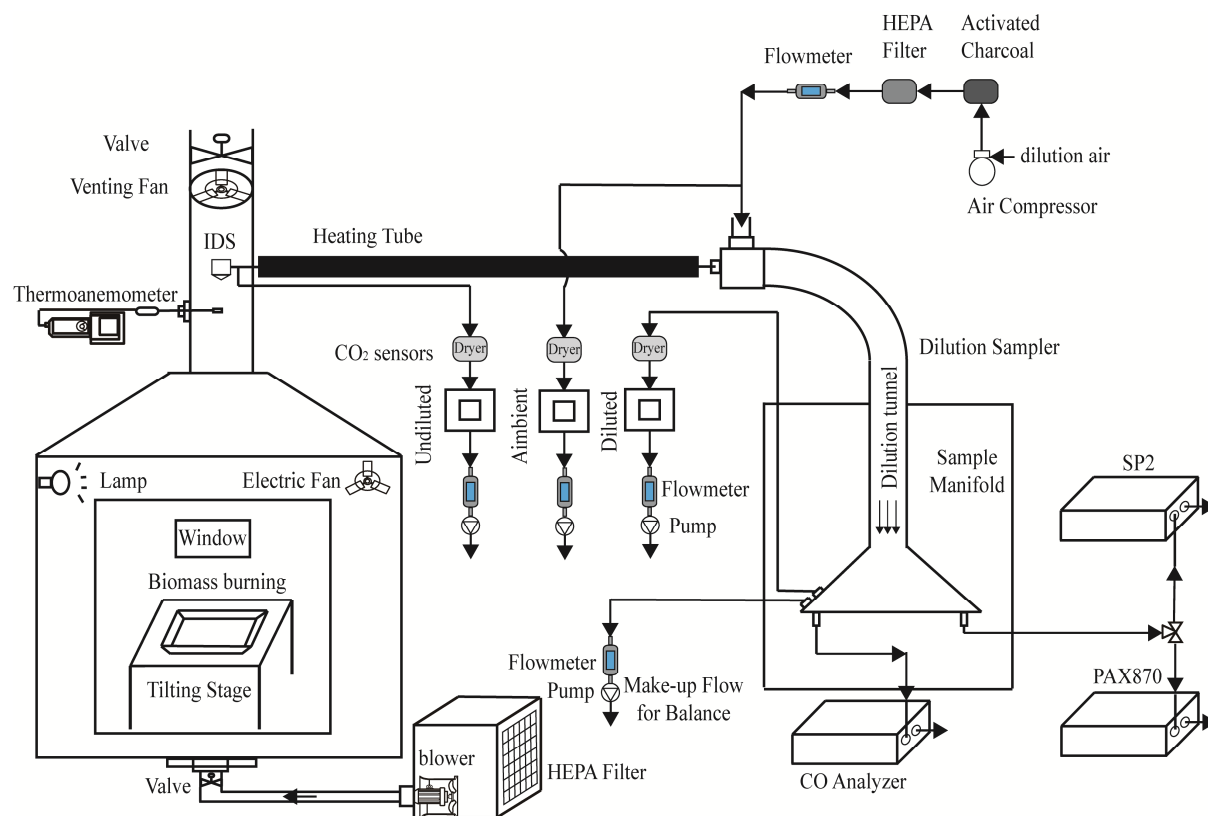
606 **Fig. 5.** Relationship between rBC mass median diameter and modified combustion
607 efficiency for five types of crop residues emissions.

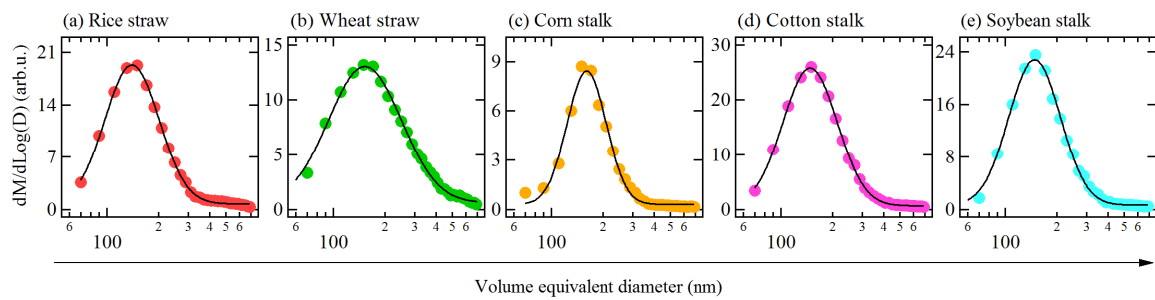
608 **Fig. 6.** Relationship between number fraction of thickly-coated rBC (F_{rBC}) and
609 modified combustion efficiency for five types of crop residues emissions.

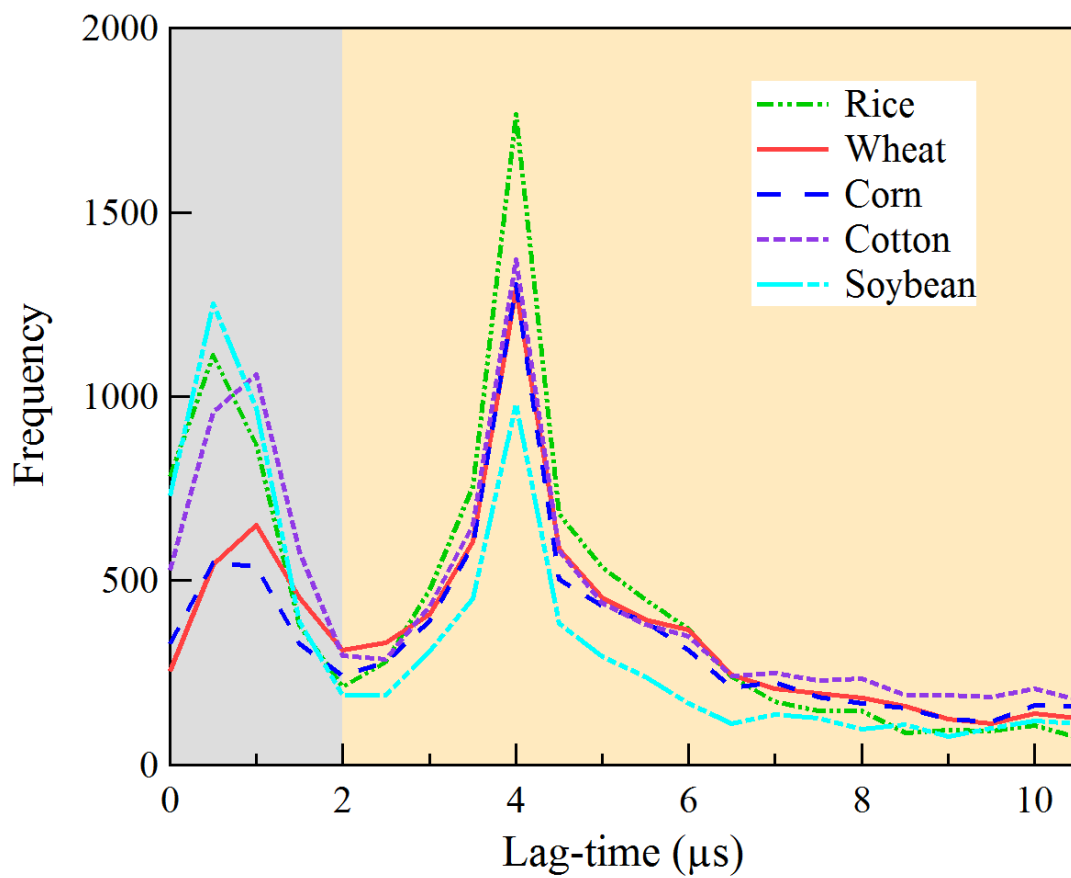
610 **Fig. 7.** Frequency distribution of rBC mass absorption cross section (MAC) for five
611 types of crop residues emissions.

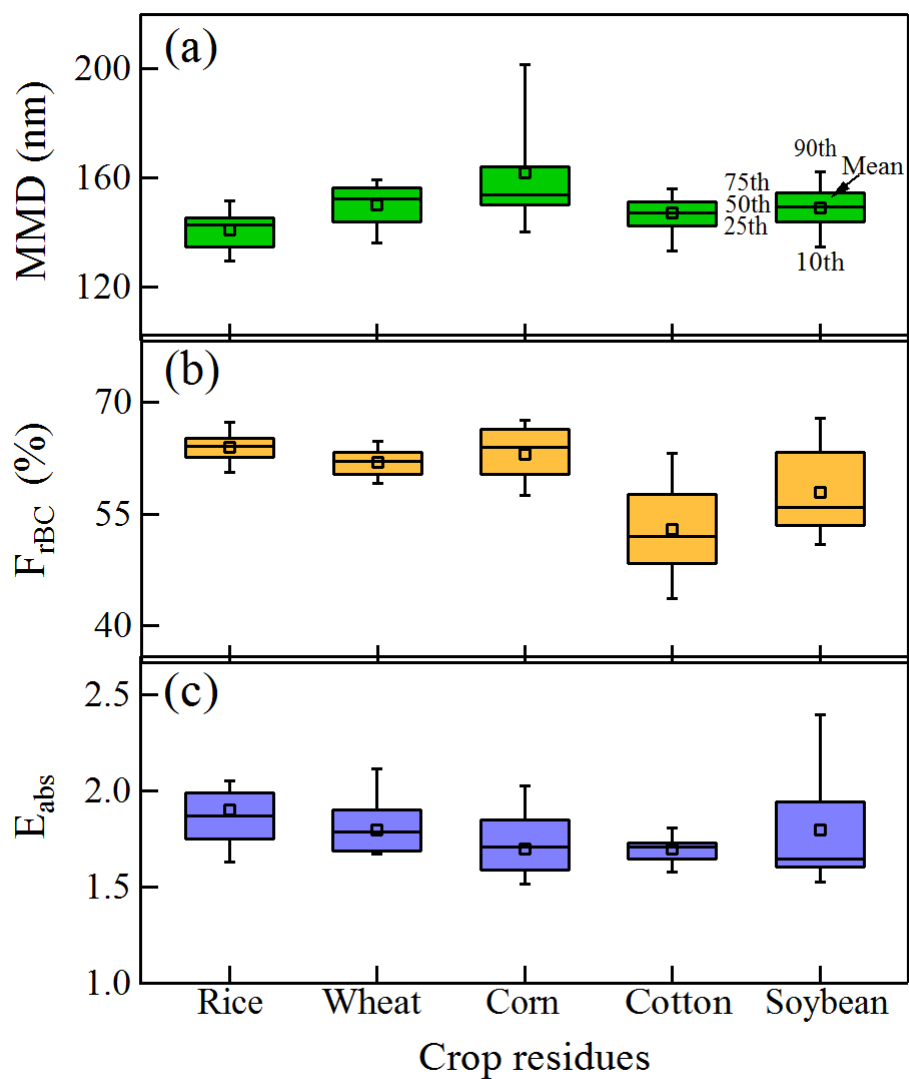
612 **Fig. 8.** Scatterplot of absorption enhancement versus (a–e) number fraction of
613 thickly-coated rBC and (f–j) rBC mass median diameter for different types of
614 crop residues emissions. The solid line fits were calculated by orthogonal
615 regression.

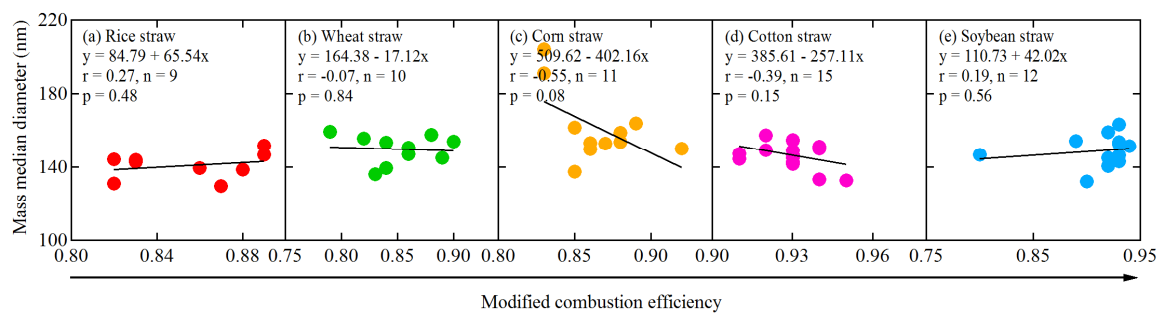
616

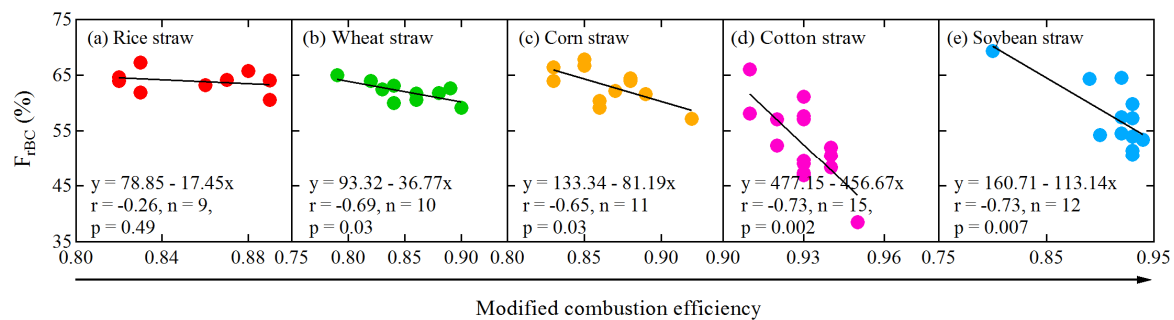


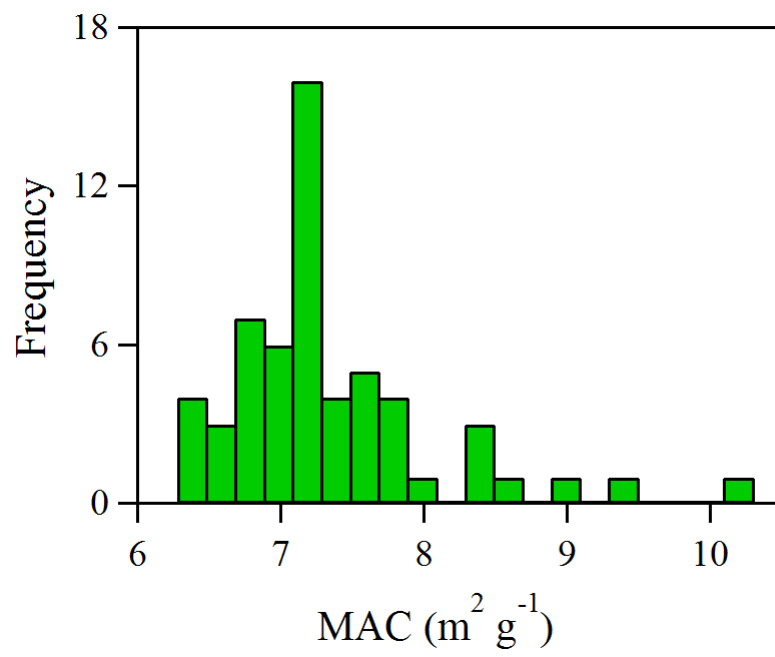


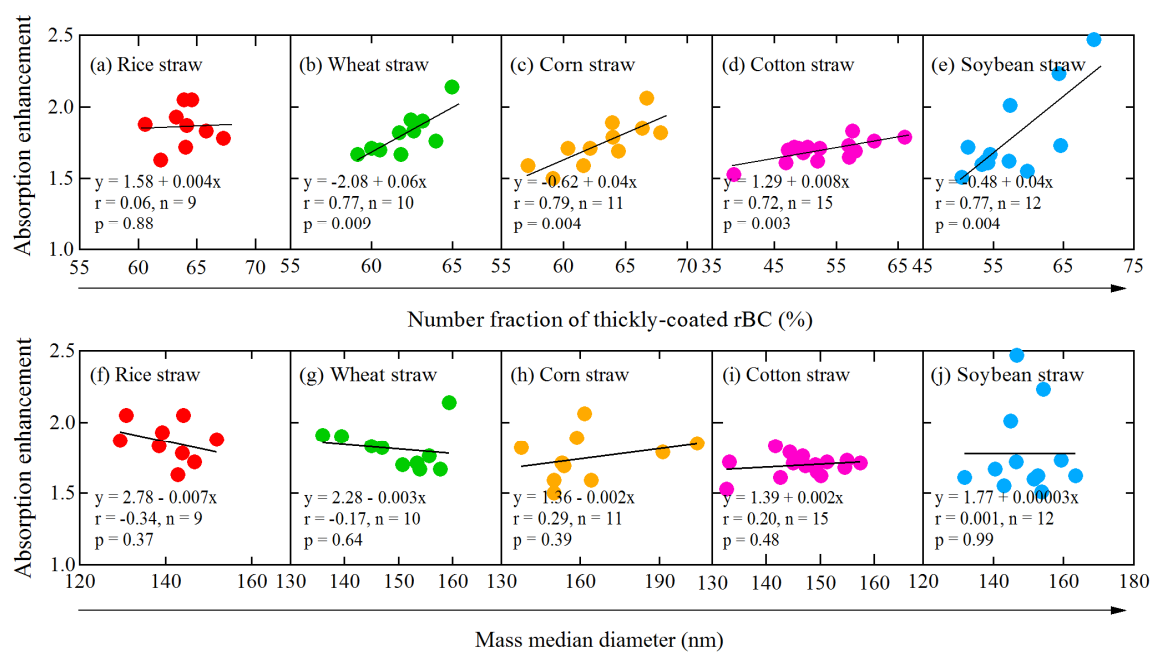












Highlights:

- Insignificant correlations were found between rBC MMDs and combustion conditions.
- The fraction of thickly-coated rBC was anti-correlated with combustion conditions.
- Large absorption enhancements were found in fresh biomass-burning emissions.